

Stability of domain walls with inflationary fluctuations under potential bias, and gravitational wave signatures

Naoya Kitajima,^{1,2} Junseok Lee,² Fuminobu Takahashi,² and Wen Yin²

¹*Frontier Research Institute for Interdisciplinary Sciences,
Tohoku University, Sendai, Miyagi 980-8578, Japan*

²*Department of Physics, Tohoku University, Sendai, Miyagi 980-8578, Japan*

Abstract

A recent study has shown that domain walls with initial inflationary fluctuations exhibit remarkable stability against population bias due to long-range correlations, challenging the claims of prior research. In this paper, we study the dynamics of these domain walls in the presence of potential bias and show that they collapse with a lifetime several times longer than that due to thermal fluctuations. This is interpreted as a difference in the average distance between domain walls, leading us to derive a new formula for the domain wall lifetime that depends on the area parameter. In addition, we compute the spectrum of gravitational waves generated by such domain walls and find that both the peak frequency and the peak abundance are lowered in a manner that depends on the area parameter. Based on these findings, we also determine the necessary degree of vacuum degeneracy for axion domain walls to explain the isotropic cosmic birefringence.

I. INTRODUCTION

Spontaneous symmetry breaking (SSB) leads to various topological defects that inherit information from high-energy physics. While the stability of individual defects is ensured by their topological nature, the stability and evolution of networks of defects are not always obvious. By studying the cosmological evolution of their network, we can learn about physics beyond the Standard Model and the evolution of the early universe. In this paper, we examine the stability of domain walls, which result from SSB of discrete Z_2 symmetry [1–3] (see Ref. [4] for reviews).

The simplest model that produces domain walls is the Z_2 model given by

$$V_0(\phi) = \frac{\lambda}{4}(\phi^2 - v^2)^2 = \frac{\lambda}{4}v^4 - \frac{1}{2}m_0^2\phi^2 + \frac{\lambda}{4}\phi^4 \quad (1)$$

with $m_0 \equiv \sqrt{\lambda}v$. Here ϕ is a real scalar field, $\lambda(> 0)$ is the quartic coupling, and there are two degenerate vacua located at $\phi = \pm v$ due to the Z_2 symmetry, $\phi \rightarrow -\phi$. Domain walls are structures that separate these two vacua, and their tension σ is given by $\sigma \sim m_0v^2$. Domain walls are known to quickly reach the scaling solution, where there is roughly one domain wall per Hubble horizon [5–12]. The energy density of domain walls following the scaling solution decreases more slowly than non-relativistic matter or radiation, and therefore eventually could dominate the universe. Then, domain walls would cause too large anisotropies in the cosmic microwave background radiation (CMB) in contradiction with observations, unless their tension satisfies the Zel’dovich bound, $\sigma \lesssim (\text{MeV})^3$ [1]. This is the cosmological domain wall problem [1, 13].

Several mechanisms have been suggested to destabilize domain walls to avoid this problem. In particular, introducing bias in the potential and/or in the initial distribution has been investigated in the literature. When a bias is introduced in the potential, domain walls collapse soon after the false vacuum pressure becomes stronger than their tension [14–18]. On the other hand, when bias is introduced in the initial distribution, which we call population bias, some studies claimed that domain walls disappear quickly for both thermal and initial inflationary fluctuations [15, 16, 19–24]. This was a common belief in this field. However, Gonzalez and three of the present authors (NK, FT, and WY) recently showed that this common belief is far from reality and that domain walls with inflationary fluctuations

as initial conditions are very stable against the population bias [25].¹ The reason for this stability is that correlations at superhorizon scales are preserved since the dynamics of the domain walls is locally governed by the random motion in the absence of potential bias. The purpose of this paper is to clarify how the stability of domain walls with initial inflationary fluctuations changes with potential bias.

Axion domain walls are an example of such domain walls with inflationary fluctuations as initial conditions [26] (see also Refs. [25, 27–40]). Axions are known to have a periodic potential and thus have domain wall solutions separating degenerate minima. Since the axion potential is stable against perturbative radiative corrections, axions naturally remain light during inflation and acquire quantum fluctuations. The recent finding of Ref. [25] implies that axions with inflationary fluctuations, which are naturally biased towards one of the vacua, could play an important cosmological role through their domain walls.

One of the interesting cosmological implications of domain walls is the generation of gravitational waves from their collapse [3, 41–51]. Recently, Murai and the present authors have for the first time calculated gravitational waves generated during the collapse of domain walls [51] and have shown that the axion domain walls coupled to QCD naturally explain the stochastic gravitational waves in the nHz range recently detected by the pulsar timing arrays. [52–55] (see also Refs. [47, 50] for the generation of nHz gravitational waves from axion domain walls). Later in this paper, we will estimate the gravitational wave spectrum for the two initial conditions, thermal and inflationary fluctuations. Especially the latter is calculated for the first time in this paper. Another is the cosmic birefringence due to axion domain walls coupled to photons [25, 37, 38, 51]; they can nicely explain the close proximity of the observed isotropic rotation angle of the CMB polarization [56, 57] to the fine structure constant, and also predict a characteristic power spectrum of the anisotropic cosmic birefringence within the reach of future CMB observations.

In this paper, we study how a network of domain walls with initial inflationary fluctuations evolves under a potential bias. We find that while these domain walls are remarkably stable against population bias, they decay under potential bias with a lifetime a few times longer than those with thermal fluctuations. We calculate the spectrum of gravitational waves

¹ The error in the past literature arose from improperly applying percolation theory to fluctuations with superhorizon-scale correlations, combined with a failure in the numerical generation of inflationary fluctuations for the initial conditions.

generated in the scaling regime of the domain walls for the two initial conditions, and show that the difference can be attributed to the area parameter for the two cases. We also derive an upper limit on the energy difference between adjacent vacua to account for cosmic birefringence with axion domain walls.

The rest of this paper is organized as follows. In Sec. II, we explain the set-up with the domain wall solution and the two representative initial conditions. In Sec. III we introduce the two types of biases, population bias and potential bias. Our numerical results are presented in Sec. IV. The gravitational wave spectrum is calculated in Sec. V. The last section is devoted to discussion and conclusions.

II. DOMAIN-WALL NETWORK

A. Set-up

The Lagrangian for a real scalar field $\phi(x)$ is given by

$$\mathcal{L} = -\frac{1}{2}\partial_\mu\phi\partial^\mu\phi - V(\phi), \quad (2)$$

where $V(\phi)$ is the potential, and we consider $V(\phi) = V_0(\phi)$ given in Eq. (1) for the moment. Later we will add an extra term that explicitly breaks the Z_2 symmetry. In the Friedmann-Lemaître-Robertson-Walker (FLRW) universe, the equation of motion of ϕ is given by

$$\ddot{\phi} + 3H\dot{\phi} - \frac{1}{a^2}\Delta\phi + \frac{\partial V}{\partial\phi} = 0, \quad (3)$$

where H is the Hubble parameter, the dot denotes the time derivative, and Δ is the Laplacian with respect to the comoving coordinate.

Throughout this paper, we consider the radiation-dominated universe with $H = 1/2t$. For later use let us define the conformal Hubble parameter \mathcal{H} and the conformal time τ ;

$$\mathcal{H} \equiv aH, \quad (4)$$

$$\tau \equiv \int_0^t \frac{dt'}{a(t')} = \sqrt{\frac{2t}{m_0}}, \quad (5)$$

where we set the scale factor equal to unity when $H = m_0$ in the last equality. With this normalization, the scale factor is given by $a(\tau) = m_0\tau$.

We assume that the scalar field ϕ initially remains near the local maximum at the origin, accompanied by some fluctuations. In the Z_2 model, this assumption is reasonable, since

the origin is a symmetry-enhanced point and can be stabilized by additional corrections such as thermal mass in the very early universe. If the field is in thermal contact with the plasma, the initial fluctuation is due to thermal fluctuations. On the other hand, if the scalar remains light during inflation and is decoupled after inflation, the fluctuation is inflationary with correlation at superhorizon scales.

Domain walls are characterized by their tension. For the Z_2 potential $V_0(\phi)$, the tension σ is given by

$$\sigma = \frac{2\sqrt{2}}{3} \sqrt{\lambda} v^3 = \frac{2\sqrt{2}}{3} \frac{m_0^3}{\lambda}. \quad (6)$$

The width of domain walls is of order m_0^{-1} , and at scales larger than the width, the properties of domain walls do not depend on details of the potential shape and are characterized only by the tension. Thus, we will be able to apply our results based on the Z_2 model to the sine-Gordon potential for the axion later in this paper.

B. Scaling solution

The energy of the domain-wall network is approximately given by the product of its area and the tension, if it is non-relativistic. Thus, once formed, domain walls move around to minimize their surface area due to their tension. When domain walls collide, they disappear, further reducing the surface area. Since the motion of domain walls tends to minimize the area only locally, the typical radius of curvature cannot significantly exceed the Hubble horizon scale. As a result, the domain-wall network is known to approach the situation where approximately one domain wall is contained within each Hubble volume. This is the so-called scaling solution, for which the (spatially averaged) energy density of the domain walls, ρ_{DW} , is given by

$$\rho_{\text{DW}} \sim \sigma H. \quad (7)$$

The scaling solution has been numerically confirmed in the literature [5–12]. However, most of the literature investigates it for white noise initial conditions corresponding to thermal fluctuations. On the other hand, Ref. [25] is the first to correctly investigate the scaling solution for inflationary fluctuations, which is discussed below.

In three-dimensional space, the scaling solution can also be expressed in terms of the

averaged area per Hubble horizon, A_{DW} , as

$$\mathcal{A}_3 \equiv \frac{A_{\text{DW}}}{H^{-2}} = \mathcal{O}(1). \quad (8)$$

Later we will numerically study the case with translation symmetry along one of the spatial directions, e.g. the z -axis, where the domain walls appear as lines in the remaining two-dimensional space. In this case, the scaling solution corresponds to

$$\mathcal{A}_2 \equiv \frac{L_{\text{DW}}}{H^{-1}} = \mathcal{O}(1), \quad (9)$$

where L_{DW} is the average length of the domain wall contained within a Hubble horizon. We call \mathcal{A}_2 and \mathcal{A}_3 as the area parameter. Note that the area parameter defined here differs from the one often defined in the literature as $\rho_{\text{DW}} = \frac{\mathcal{A}\sigma}{t}$ [46]. When the motion of domain walls is non-relativistic, we have $\mathcal{A}_3 \approx 2\mathcal{A}$ in the radiation-dominated universe. Note that \mathcal{A}_3 is defined in terms of area, while \mathcal{A} is defined using energy density.

The exact value of the $\mathcal{O}(1)$ constant on the RHS of the above equations depends on the initial conditions [25]. For the two initial conditions we introduce in the next subsection, they differ by a factor of about 2. This difference actually comes from the large-scale correlation of the domain-wall network encoded by the initial condition. We emphasize here that the energy density or surface area (or length) is a spatially averaged quantity and does not capture well the global properties of the domain-wall network. We need to compute the power spectrum of the scalar field to directly see the global structure of the domain-wall network.

C. Initial conditions

Scalar field fluctuations can be generated from a variety of sources, but typical ones are thermal and inflationary fluctuations. In this paper, we consider these two initial fluctuations, but it is straightforward to perform other types of fluctuations.

To represent the initial fluctuations, it is convenient to use their two-point correlation function or power spectrum;

$$\langle \phi(\mathbf{k})\phi(\mathbf{k}') \rangle = (2\pi)^d \delta^{(d)}(\mathbf{k} + \mathbf{k}') P(k), \quad (10)$$

where $\phi(\mathbf{k}) = \int d^d \mathbf{x} e^{-i\mathbf{k}\cdot\mathbf{x}} \phi(\mathbf{x})$ is the Fourier mode of $\phi(\mathbf{x})$, $d = 2, 3$ is the spatial dimension, and $P(k)$ is the power spectrum with k being $|\mathbf{k}|$. Here, we have assumed statistical isotropy,

which implies that the power spectrum depends solely on the momentum modulus. For the sake of brevity, we have omitted the explicit time dependence in our notation.

The variance of fluctuations in real space is related to the power spectrum as

$$\langle \phi^2(\mathbf{x}) \rangle = \int \frac{d^d \mathbf{k}}{(2\pi)^d} P(k) = \int d \ln k \mathcal{P}(k), \quad (11)$$

where $\mathcal{P}(k)$ is the reduced power spectrum, and it is given by $\mathcal{P}(k) = k^2 P(k)/2\pi$ for $d = 2$, and $\mathcal{P}(k) = k^3 P(k)/2\pi^2$ for $d = 3$.

The vacuum fluctuation of a scalar field with mass m in the flat Minkowski space is given by $\langle \phi(\mathbf{k})\phi(\mathbf{k}') \rangle = \frac{1}{2\sqrt{k^2+m^2}} \delta^{(d)}(\mathbf{k} + \mathbf{k}')$ with some ultraviolet cutoff. On scales larger than m^{-1} , the power spectrum is independent of \mathbf{k} . This is the same as white noise, which is defined to have a constant power spectrum, $P(k) = \text{const.}$, or equivalently, $\mathcal{P}(k) \propto k^d$. In real space, white noise is often implemented by generating the random field values at each lattice site. Similar fluctuations are obtained for thermal fluctuations on scales larger than the thermal correlation length. The white noise fluctuation is a plausible choice for the initial condition if there were no correlations at superhorizon scales because, in that case, the field value averaged over the Hubble horizon should follow the random distribution. In most of the literature, the white noise initial condition has been adopted in the numerical lattice calculations of the topological defects. This choice of the initial fluctuation is in line with the spirit of the Kibble mechanism [2]. In the following, thermal fluctuation and white noise are used interchangeably.

On the other hand, the initial fluctuations at superhorizon scales could have non-trivial correlations. This is the case if the corresponding scalar is light during inflation. Then, it acquires quantum fluctuation of order the Hubble parameter during inflation, H_{inf} , leading to the (almost) scale-invariant power spectrum,

$$\mathcal{P}(k) = \left(\frac{H_{\text{inf}}}{2\pi} \right)^2 \quad (12)$$

at $k \lesssim aH = \mathcal{H}$. Compared to the white noise fluctuations, it is not suppressed at large scales, implying that the domain-wall network has correlations at superhorizon scales. This initial inflationary fluctuation was correctly implemented for the first time in numerical lattice simulations of domain walls in Ref. [25], where it was found that the structure of the domain-wall network as well as its subsequent evolution is completely different from that with the white noise initial condition. In the following, inflationary fluctuation refers to this scale-invariant fluctuation.

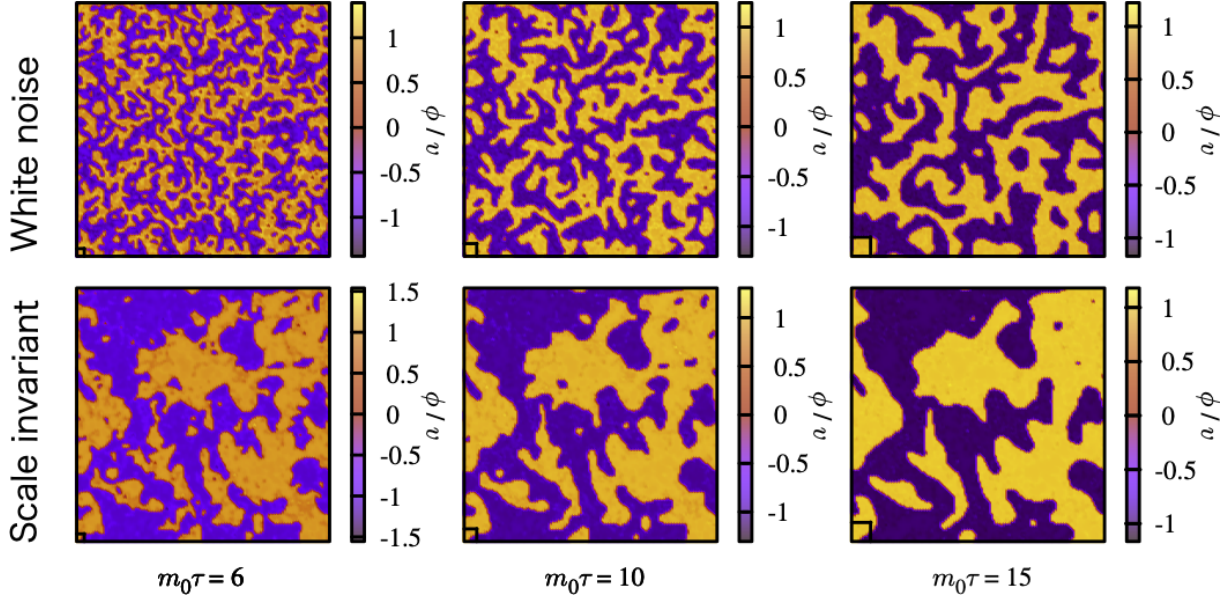


Fig. 1: The snapshots of the domain wall distributions at different times $\tau = 6, 10, 15/m_0$ from left to right, where the initial conditions are provided by either the white noise (top) or the scale-invariant fluctuations (bottom). No bias is introduced. Approximately $67^2, 20^2, 13^2$ Hubble horizons are contained in order of increasing time. The size of the Hubble horizon is indicated by the small box in the lower left of each plot. The simulations are performed on an 8192^2 comoving lattice. The color scheme represents the field value normalized by v .

In Fig. 1 we show snapshots of the domain-wall network at different times for the white noise (top) and the inflationary fluctuations (bottom). It is evident that the global network structure differs significantly between these cases. In particular, in the case of inflationary fluctuations, the global structure of the domain-wall network remains preserved as it undergoes coarse-graining over time. The persistent stability of this global structure serves as the underlying reason for the robustness of domain walls with inflationary fluctuations [25].

III. DESTABILIZING DOMAIN WALLS WITH BIASES

The stability of domain walls is ensured by their topological nature and, in the case of the Z_2 model, by the Z_2 symmetry. Since they follow the scaling solution, their energy density decreases more slowly than that of radiation or non-relativistic matter. Consequently, domain walls eventually come to dominate the energy density of the universe, leading to an

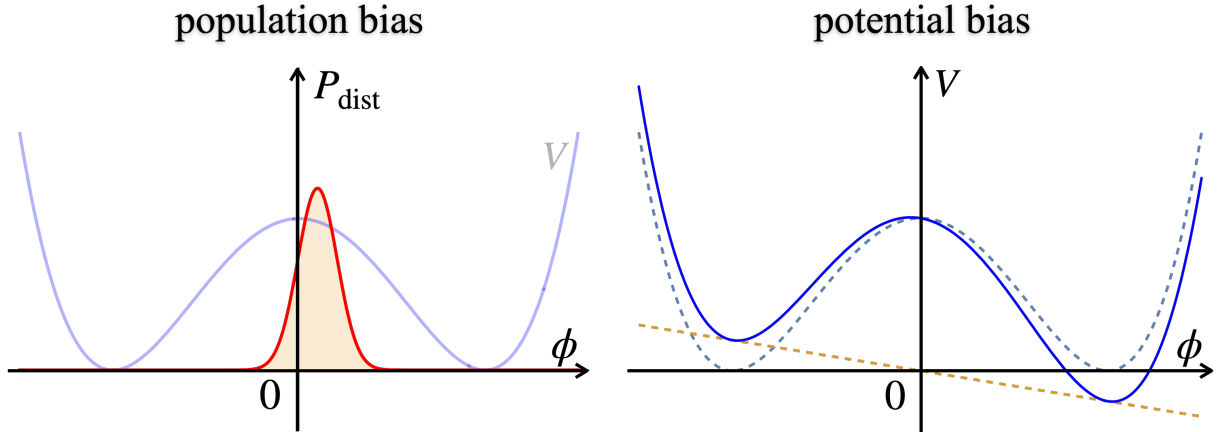


Fig. 2: Illustration of the two biases introduced to destabilize the domain-wall network. (Left) Population bias: The initial distribution of the scalar field is biased toward one of the vacua, resulting in an uneven population of vacua. (Right) Potential bias: An explicit Z_2 breaking term lifts the degeneracy of the two vacua, leading to the preferential motion of the domain walls.

unwanted inhomogeneity that contradicts observations. This is known as the cosmological domain wall problem [1]. To avoid this problem, there are two possibilities: either the domain wall tension must be less than $\sim (\text{MeV})^3$, or the domain-wall network must become unstable and decay before reaching dominance.

In this study, we explore the latter possibility by considering the breaking of the Z_2 symmetry. Two biases can be introduced to render the domain-wall network unstable: the initial population bias and the potential bias, as shown in Fig. 2. The left panel shows the initial population bias, which corresponds to a biased distribution of the scalar field in the initial state. As a result, one vacuum occupies a larger or smaller volume than the other, causing the domain walls to move in a way that amplifies the bias over time due to their tension. On the other hand, the right panel shows the potential bias, which affects the dynamics of the domain walls in a more intuitive way. The potential bias induces negative pressure in the false vacuum, causing the domain walls to move toward it. When the pressure acting on the walls exceeds their tension, the domain walls progressively converge toward the false vacuum. Thus, for the population bias, the local behavior of the domain walls is the same as under unbiased conditions. In contrast, the potential bias introduces a preferred direction of motion that affects the domain wall dynamics on both local and global scales.

The effects of both biases on the domain-wall network have been extensively studied in the literature for two different initial conditions: white noise and inflationary fluctuations. Previous studies have shown that both biases contribute to the rapid decay of the domain-wall network, with the initial population bias having a particularly strong impact in both cases [15, 16, 19–24]. However, it is crucial to note that previous numerical simulations did not properly incorporate the initial inflationary fluctuations, resulting in a substantial underestimation of correlations at the superhorizon scales. Also, the use of percolation theory in the past literature to analyze inflationary fluctuations has been misguided due to the overlooked long-range correlations, which fundamentally invalidate its application.

A recent study by Gonzalez and some of the present authors [25] has shed new light on this issue. Surprisingly, the domain-wall network with initial inflationary fluctuations was found to be remarkably stable to the initial population bias, contrary to the prevailing understanding in the community. This unexpected robustness can be attributed to the presence of correlations at superhorizon scales, as shown in Fig. 1. Motivated by these findings, the main objective of this paper is to investigate the stability of the domain-wall network with the initial inflationary fluctuations in the presence of the potential bias.

As a specific example of the potential bias, we introduce a linear term;

$$V(\phi) = V_0(\phi) + \delta V(\phi), \quad (13)$$

$$\delta V(\phi) = -\epsilon\lambda v^3\phi \quad , \quad (14)$$

where $V_0(\phi)$ respects the Z_2 symmetry, while the linear term δV explicitly breaks the Z_2 symmetry. Here ϵ denotes a dimensionless parameter that controls the magnitude of the potential bias, and we assume

$$\epsilon \geq 0 \quad (15)$$

without loss of generality.

The linear term δV induces a pressure on the wall toward the false vacuum, and it is approximately given by the potential difference between two local minima ΔV :

$$p \approx \Delta V \approx 2\epsilon\lambda v^4 = \frac{2\epsilon m_0^4}{\lambda}. \quad (16)$$

This can be derived by taking the time derivative of the momentum of the wall, which is estimated by the integral of the stress-energy tensor along a line perpendicular to the wall. This pressure p affects the dynamics of the domain wall as it competes with the tension due

to the curvature of the wall. When the domain walls are in the scaling regime, the force due to tension can be approximated by $\sigma/R \sim \sigma H$, where $R \sim H^{-1}$ is a typical curvature radius.

Lastly, let us comment on a subtle point. The introduction of a linear term as a potential bias can shift the position of the local maximum away from the origin. Consequently, if we were to consider initial fluctuations around the origin in the presence of a linear term, we would be introducing a population bias as well. Since our primary focus is to examine the impact of potential bias on the evolution of the domain-wall network, we will consider fluctuations centered around the local maximum in our numerical calculations. This approach aims to minimize the effect of any secondary population bias. In the present set-up, the position of the local maximum ϕ_{\max} is given by

$$\phi_{\max} \simeq -(\epsilon + \epsilon^3 + 3\epsilon^5)v, \quad (17)$$

and we ensure that the ensemble average of the initial scalar field values is equal to ϕ_{\max} .

IV. LIFETIME OF DOMAIN WALLS UNDER BIASES

A. Set-up for numerical simulations

We have numerically solved the equation of motion (3) on the two-dimensional N_{grid}^2 lattice with $N_{\text{grid}} = 8192$ or 16384 , using the leap-frog method. The comoving size of lattice box L_{box}^2 is set to be $L_{\text{box}}^2 = (64\pi/m_0)^2$. All simulations start at the initial conformal time $\tau_i = 1/m_0$ where H is equal to m_0 . The parameters we used in simulations are shown in Table I.

As explained in Sec. II, we compare the cases of two types of initial fluctuations, the white noise and the scale-invariant fluctuations. For the numerical calculations, we choose the momentum space to set the initial distributions, because it is easy to handle the wavenumber dependence. The white noise fluctuation is generated by assigning the Gaussian distributed random number to each discretized momentum lattice site. On the other hand, the scale-invariant fluctuation can be generated by assigning the Gaussian distributed random number weighted by some power of the comoving wavenumber k on the momentum space, i.e. k^{-1} for 2D and $k^{-3/2}$ for 3D. For both cases, we introduce the ultraviolet cutoff k_{UV} as the Hubble scale, $k_{\mathcal{H}} = 2\pi\mathcal{H}$, for the initial condition to suppress the gradient energy and make

the system easy to get to the scaling solution. Note that the fluctuations are normalized in different ways. In the white noise case, the initial fluctuations are normalized so that the standard deviation in the real space, $\sqrt{\langle(\phi - \langle\phi\rangle)^2\rangle}$, is equal to $0.1v$. On the other hand, we set $\sqrt{\mathcal{P}(k)}$ to $0.1v$ in the case of scale-invariant fluctuation.² This is because the fluctuations are accumulated in real space for the scale-invariant fluctuation, and the variation in real space depends logarithmically on the box size. The initial conditions of Fig. 1 are generated this way.

Let us discuss some subtleties about the field variance in real space in the case of inflationary fluctuations. As previously mentioned, the variance increases logarithmically as the box size expands. Once the integral $\int d\ln k \mathcal{P}(k) \gtrsim v^2$, the quartic term becomes important in the Z_2 model, and at some point, the scalar is no longer sufficiently light. This constrains the range of the scalar fluctuations to a finite range. Let us consider what happens if the field value of ϕ is much larger than v , but its effective mass squared $\sim V''(\phi)$ is still smaller than the Hubble parameter. In such a case we can adopt the inflationary fluctuations. When the Hubble parameter becomes comparable to the effective mass after inflation, ϕ starts to oscillate with an amplitude much larger than v and can fall into either a positive or negative vacuum. Thus, as the size of the box increases, positive and negative vacua are randomly populated at sufficiently large scales. Consequently, the statistical properties of the fluctuations gradually transition from inflationary to thermal as one moves to larger scales. This transition can be interpreted as the restoration of the Z_2 symmetry due to the effective mass arising from self-coupling, which only becomes important at large scales. In this limit, the resulting domain-wall network with inflationary fluctuations is realized only in rare regions of the large box. We have confirmed this transition numerically. However, it occurs only when considering a case of $\int d\ln k \mathcal{P}(k) \gtrsim v^2$, and it also depends on the potential shape beyond the potential minima. In fact, such a transition does not occur in the case of the cosine potential, and other vacua are populated. In this case, the field correlation remains on a large scale. In the following, we focus on a regime where the variance of the scalar field is sufficiently small so that the evolution of the domain-wall network does not depend on the potential shape beyond the potential minima.³

² In the real space, this corresponds to $\sqrt{\langle(\phi - \langle\phi\rangle)^2\rangle} \simeq 0.23v$.

³ This transition can be used to suppress isocurvature perturbations of ϕ particles. As we will discuss later, if ϕ particles produced from the collapse of the domain walls with inflationary fluctuations contribute to

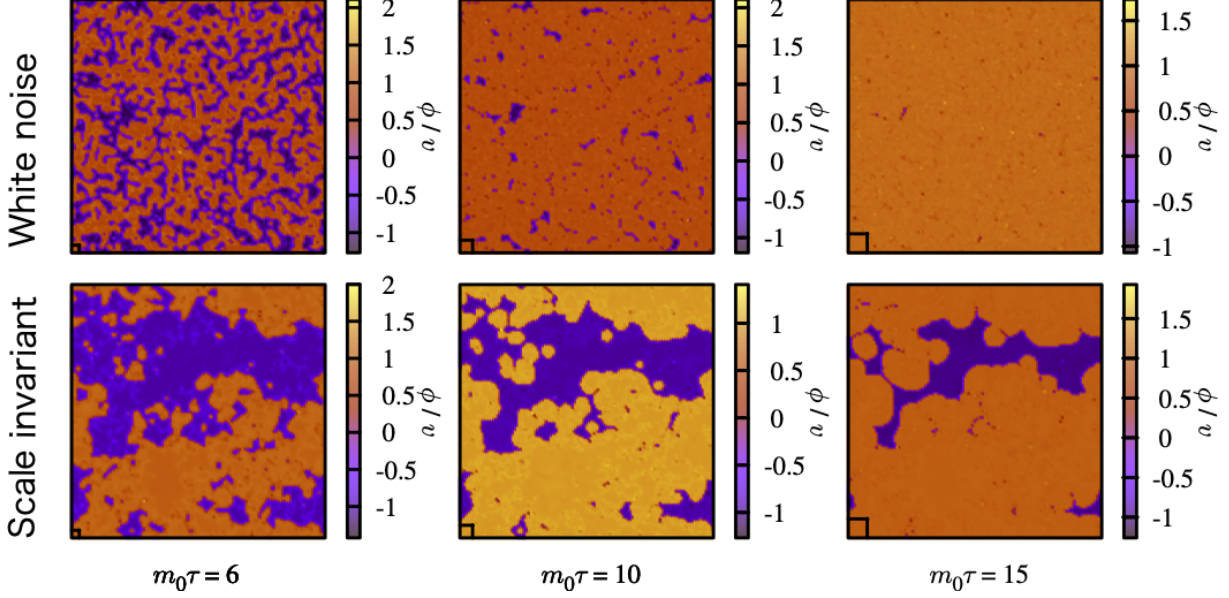


Fig. 3: Same as Fig. 1 but with the potential bias, $\epsilon = 0.05$.

In simulations of domain walls, two distinct physical scales emerge: the Hubble length H^{-1} and the wall width $\sim m_0^{-1}$. As the universe expands, the former scales as τ^2 , while the latter stays constant. To ensure the validity of our results, the simulation box should contain more than $\mathcal{O}(1)$ Hubble horizons,

$$\left(\frac{a(\tau)L_{\text{box}}}{H(\tau)^{-1}}\right)^2 = \left(\frac{L_{\text{box}}}{\tau}\right)^2 \gtrsim \mathcal{O}(1), \quad (18)$$

throughout the simulation. Simultaneously, the lattice spacing given by $a(\tau)L_{\text{box}}/N_{\text{grid}}$ must be finer than the physical wall width $\sim m_0^{-1}$,

$$\frac{m_0^{-1}}{a(\tau)L_{\text{box}}/N_{\text{grid}}} = \frac{N_{\text{grid}}}{m_0^2 L_{\text{box}} \tau} \gg \mathcal{O}(1), \quad (19)$$

to prevent the momentum of the domain walls from being artificially truncated. Note that the actual width of the moving walls is thinner due to the Lorentz contraction. Thus, we must use sufficiently fine grid spacing to resolve the wall width, especially in the case of inflationary fluctuations.

dark matter, isocurvature perturbations may become too large. However, by considering the transition to white noise at large scales discussed here, the isocurvature perturbations of ϕ can be suppressed.

Case	Fluc.	ϵ	N_{grid}^2	$m_0\tau_{\text{end}}$	Realization	Case	Fluc.	ϵ	N_{grid}^2	$m_0\tau_{\text{end}}$	Realization
(a-1)	WN	0	8192^2	15	100	(b-1)	SI	0	8192^2	15	100
(a-2)	WN	0.0004	16384^2	30	40	(b-2)	SI	0.0008	16384^2	30	40
(a-3)	WN	0.0008	16384^2	30	10	(b-3)	SI	0.001	16384^2	30	40
(a-4)	WN	0.001	16384^2	30	10	(b-4)	SI	0.0015	16384^2	30	10
(a-5)	WN	0.0015	16384^2	30	10	(b-5)	SI	0.002	16384^2	30	10
(a-6)	WN	0.002	16384^2	30	10	(b-6)	SI	0.003	8192^2	15	100
(a-7)	WN	0.003	8192^2	15	100	(b-7)	SI	0.005	8192^2	15	100
(a-8)	WN	0.005	8192^2	15	100	(b-8)	SI	0.008	8192^2	15	100
(a-9)	WN	0.008	8192^2	15	100	(b-9)	SI	0.01	8192^2	15	100
(a-10)	WN	0.01	8192^2	15	100	(b-10)	SI	0.02	8192^2	15	100
(a-11)	WN	0.02	8192^2	15	100	(b-11)	SI	0.03	8192^2	15	100
(a-12)	WN	0.03	8192^2	15	100	(b-12)	SI	0.05	8192^2	15	100
(a-13)	WN	0.05	8192^2	15	100						

Table I: Setting of parameters used in simulations. NW indicates the white noise case and SI indicates the scale-invariant case. All cases were run in the comoving lattice containing $(m_0 L_{\text{box}})^2 = (64\pi)^2$ Hubble horizons, and in each case, the results are averaged over the number of realizations. All simulations were stopped at $m_0\tau_{\text{end}}$. In the cases with small biases, such as (a-2)-(a-6) and (b-2)-(b-5), longer simulation times are required due to their long lifetimes, so we use a larger N_{grid} .

B. Evolution of the area parameter

First, we show in Fig. 3 the evolution of the domain-wall network under the influence of a potential bias. The snapshots are taken at $m_0\tau = 6, 10$, and 15. With time, the pressure generated by the potential bias becomes more relevant, as the force from the tension decreases due to the cosmic expansion. It can be seen that the closed domain walls surrounding the true vacuum regions tend to expand outward, and the system is gradually covered by true vacuum regions.

Next, we examine the time evolution of \mathcal{A}_2 , which quantifies the average domain wall

area within a Hubble patch, based on our 2D lattice simulations.⁴ We evaluate the length of walls by counting the number of lattice points on which $(\phi - \phi_{\max})$ flips its sign and multiplying the lattice spacing where ϕ_{\max} is the field value for the local maximum. In Fig. 4, each trajectory corresponds to a different bias parameter ϵ ranging from 0 to 0.05, where the dashed line represents $\epsilon = 0$ and the solid lines represent cases with non-zero bias.

In the case of $\epsilon = 0$, the domain wall area follows the scaling law expressed in Eq. (9) for $\tau \gtrsim 4/m_0$, except for a slight increase due to the finite resolution of the lattice [25].⁵ In the case of the scale-invariant fluctuations, this increase is more pronounced when potential biases are present. We believe that this increase is mainly due to the outward expansion of the domain walls surrounding the true vacuum regions. Note that this should work only when there is plenty of space for the true vacuum regions to expand, which explains why we do not observe a pronounced increase in the white noise case. That is to say, in the white noise case, such expanding true vacuum regions soon coalesce, reducing the area parameter. On the other hand, in the scale-invariant case, there are always large voids due to the large-scale correlations, where the true vacuum regions continue to expand, increasing the area parameter. In this sense, the area parameter \mathcal{A}_2 is not a good measure of the lifetime of the domain-wall network, especially for the scale-invariant case, although it has been the focus of most of the previous literature. This is one of the reasons why we use the volume fraction of the false vacuum to study the lifetime, which will be explained next.

C. Volume fraction of the false vacuum

1. Evolution with potential bias

Let us introduce a volume fraction of the false vacuum, r_V , defined by

$$r_V \equiv \frac{V_-}{V_+ + V_-}, \quad (20)$$

where V_+ (V_-) is the volume of regions with positive (negative) values of $\phi - \phi_{\max}$ since the local maximum is slightly shifted by the linear potential bias. Note that in our setup

⁴ In our 2D simulations, we often use common three-dimensional terminology; the term ‘volume’ should be understood as ‘area’. Similarly, when we mention the area parameter, it should be interpreted as ‘length’.

⁵ This was further confirmed in Ref. [58], where it was shown that the area parameter converges to a constant as both the spatial resolution and the box size are increased.

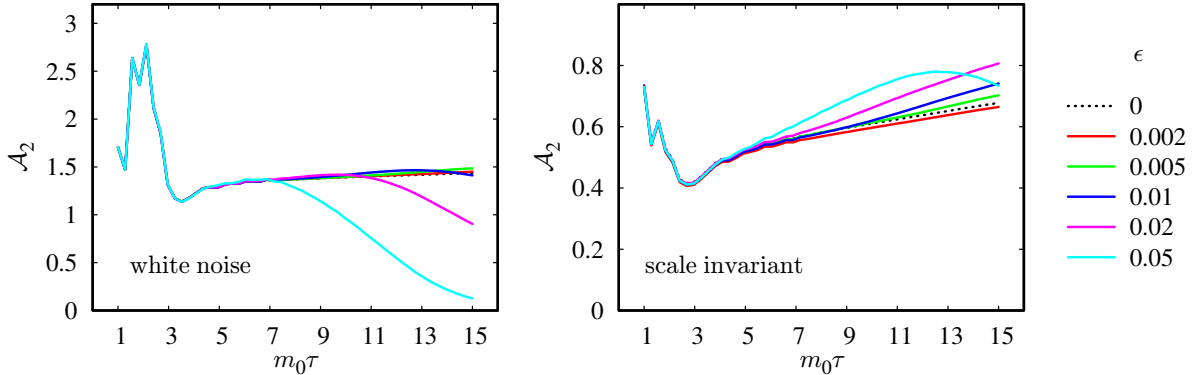


Fig. 4: The time evolution of the area parameter $\mathcal{A}_2 = L_{\text{DW}}/H^{-1}$ with the bias parameter $\epsilon = 0 - 0.05$ for the white noise (left) and scale-invariant (right) initial fluctuations, based on 100 simulations. Each line represents a different bias parameter $\epsilon = 0 - 0.05$. The dotted lines are for the case of $\epsilon = 0$.

the negative vacuum becomes the false vacuum in the presence of the potential bias. The volume fraction has an advantage over the area parameter in that, averaged over realizations, it shows a monotonically decreasing function of time, which can be nicely fitted by an exponential function.

In Fig. 5 we show the time evolution of r_V for the white noise and scale-invariant initial fluctuations, varying the potential bias parameter ϵ . It can be seen that, unlike the area parameter, r_V decreases progressively with time for all cases, and its dependence on ϵ is also monotonic. Here, the width of the bands corresponds to the variance over realizations. The bands for the scale-invariant cases are wider than for the white noise case due to the large variance of the structure at large scales. The dashed lines are obtained from the numerical fit assuming the following dependence,

$$r_V \propto \exp \left[- \left(\frac{\tau - \tau'}{\tau_{\text{decay}}} \right)^2 \right]. \quad (21)$$

The range for the fit is $\tau = 6 - 30/m_0$ for the cases (a-2)-(a-6) and (b-2)-(b-5) in Table I, and $\tau = 6 - 15/m_0$ otherwise. Note that $\tau = 6/m_0$ is the time after which the scaling solution is reached when $\epsilon = 0$. The numerical fitting results are summarized in the Table II.

In Table II, a notable transition in behavior is observed at large values of ϵ . This transition can be attributed to the limitations of the lattice resolution. In fact, as ϵ increases, the false

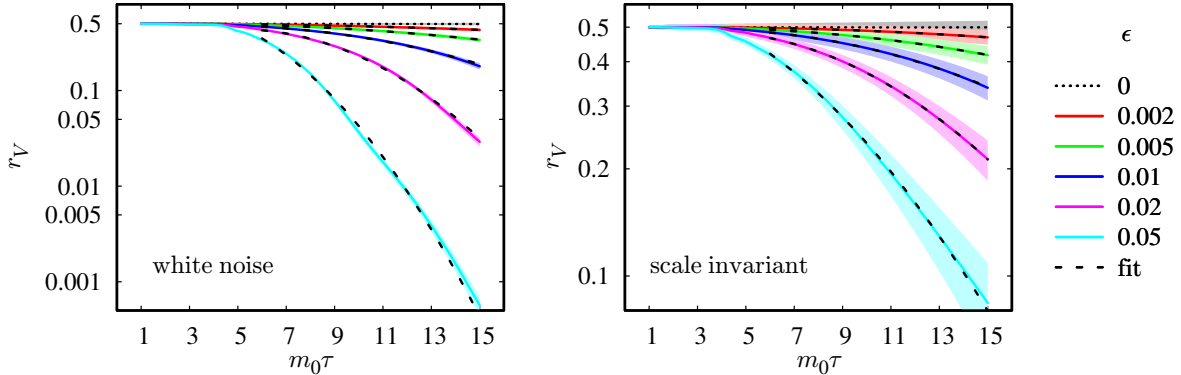


Fig. 5: The time evolution of the false vacuum volume fraction with the bias parameter $\epsilon = 0 - 0.05$ for the white noise (left) and scale-invariant (right) initial fluctuations. The dotted lines are for $\epsilon = 0$. The colored band shows the variance across realizations. The dashed lines correspond to the numerical fit assuming the functional form of Eq. (21). See the main text for details.

vacuum region shrinks more rapidly, driving the domain walls to relativistic velocities earlier. In cases (a-11) to (a-13), as well as (b-11) and (b-12), an increase in the wall width at late times was observed despite the acceleration due to the large potential bias. We consider this because the lattice spacing is insufficient to resolve the Lorentz-contracted wall width.⁶

In Fig. 6 we also plot the results from Table II. It is clear from the left panel of the figure that, given a bias, the lifetime for the scale-invariant fluctuations is longer than for the white noise fluctuations. We can also see from the left panel that the lifetime τ_{decay} scales roughly as $\epsilon^{-1/2}$ for both types of initial fluctuations, except for large values of ϵ as mentioned above. This dependence on the bias can be understood as follows. The domain walls start to move towards the false vacuum when the pressure due to the bias becomes comparable to the tension force;

$$\sigma H_{\text{eq}} = p, \quad (22)$$

where the subscript ‘eq’ implies that it is evaluated when the above equality is met. During

⁶ In our numerical simulations, the (normalized) wall width is estimated as $n_{\text{spread}}/n_{\text{flip}}$, where n_{spread} is a number of grid points whose field value is in the range of $|\phi - \phi_{\text{max}}| < v \tanh \frac{1}{2\sqrt{2}} \simeq 0.34v$ and n_{flip} is the number of cells where the field value $(\phi - \phi_{\text{max}})$ flips its sign.

ϵ	white noise		scale-invariant	
	$m_0\tau_{\text{decay}}$	$m_0\tau'$	$m_0\tau_{\text{decay}}$	$m_0\tau'$
0.0004	88.11 ± 0.55	1.23 ± 0.17		
0.0008	54.68 ± 0.18	-0.35 ± 0.10	75.84 ± 0.36	2.53 ± 0.13
0.001	50.81 ± 0.26	2.82 ± 0.13	62.33 ± 0.24	3.40 ± 0.10
0.0015	37.96 ± 0.26	2.36 ± 0.17	50.34 ± 0.15	3.66 ± 0.08
0.002	30.69 ± 0.34	3.38 ± 0.24	41.18 ± 0.35	3.67 ± 0.22
0.003	28.66 ± 0.10	1.52 ± 0.06	39.58 ± 0.16	2.44 ± 0.06
0.005	20.48 ± 0.18	2.37 ± 0.12	29.53 ± 0.16	2.65 ± 0.08
0.008	13.73 ± 0.17	3.59 ± 0.14	21.67 ± 0.14	3.16 ± 0.09
0.01	11.31 ± 0.15	4.10 ± 0.14	18.98 ± 0.14	3.48 ± 0.09
0.02	6.10 ± 0.08	5.11 ± 0.10	12.74 ± 0.04	3.43 ± 0.04
0.03	4.97 ± 0.05	4.50 ± 0.09	11.13 ± 0.06	2.49 ± 0.07
0.05	4.81 ± 0.13	1.89 ± 0.38	11.17 ± 0.19	-1.02 ± 0.35

Table II: The summary of the fitting parameters τ_{decay} and τ' in Eq. (21) for the white noise and scale-invariant fluctuations, and various potential biases. Some of the corresponding fit curves are depicted in Fig. 5. Note that the errors are the asymptotic standard errors for fitting, not the variance across the realizations. The horizontal lines separate the strongly biased cases in which the lattice cannot resolve the domain walls well because of the Lorentz contraction. See the main text.

the radiation-dominated era, this leads to

$$(m_0\tau_{\text{decay}})^2 \sim (m_0\tau_{\text{eq}})^2 = \frac{m_0\tau_i}{\epsilon}, \quad (23)$$

and thus $\tau_{\text{decay}} \propto \epsilon^{-1/2}$. This is the standard estimate of the lifetime of domain walls. However, we note that the condition (22) determines the time when the domain wall starts to decay, and it takes some more time for the walls to disappear completely [49, 59, 60].

The difference between the two different initial conditions can be interpreted as arising from the global structure of the domain-wall network. To see this, in the right panel of Fig. 6 we show the dependence of the lifetime on $\bar{\mathcal{A}}_2\epsilon$, where $\bar{\mathcal{A}}_2$ represents the area parameter in the absence of the potential bias, and the value of $\bar{\mathcal{A}}_2$ for the white noise and scale-invariant initial conditions is approximately 1.4 and 0.7 at $\tau = \tau_{\text{end}}$, respectively. It can be seen that

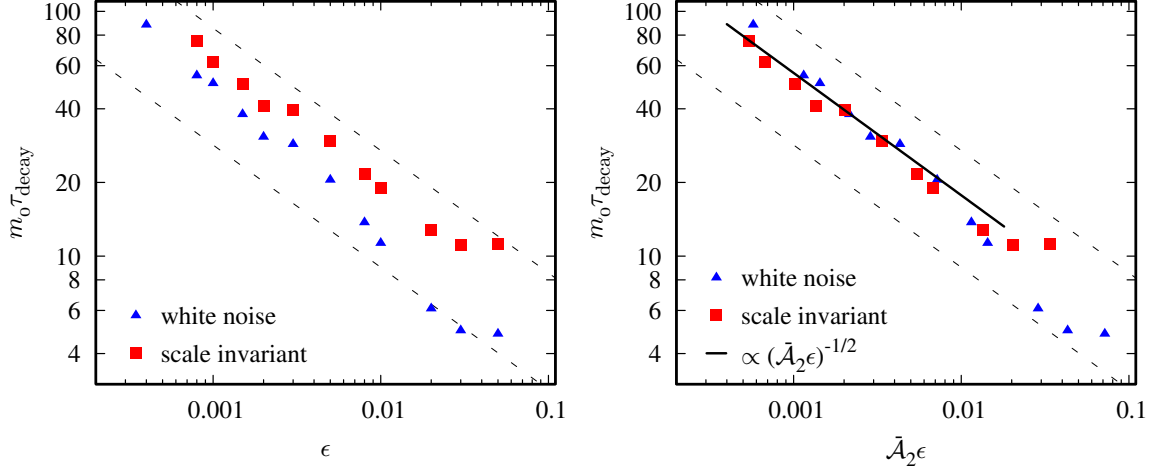


Fig. 6: The dependence of the false vacuum lifetime on the potential bias parameter ϵ (left) and $\bar{\mathcal{A}}_2\epsilon$ (right). The blue triangles are for the white noise fluctuations and the red squares are for the scale-invariant fluctuations. The gray dashed lines $\propto \epsilon^{-1/2}$ are shown for the guidance of the eyes. In the right panel, the black solid line is the numerical fit to the combined results with $\epsilon \leq 0.01(0.02)$ for the white-noise (scale-invariant) fluctuations.

the numerical results for the two cases more or less agree when plotted as a function of $\bar{\mathcal{A}}_2\epsilon$, except for very large values of ϵ . Using the following ansatz,

$$m_0\tau_{\text{decay}} = \frac{\alpha}{\sqrt{\bar{\mathcal{A}}_2\epsilon}}, \quad (24)$$

we find that the numerical fit to the combined data with weak bias shown above the horizontal line in Table. II ($\epsilon \leq 0.01(0.02)$ for the white-noise (scale-invariant) fluctuations) leads to $\alpha = 1.77 \pm 0.05$. For convenience, let us summarize our numerical results on the lifetime in terms of the cosmic time instead of the conformal time as follows:

$$t_{\text{decay}} \simeq t_{\text{eq}} \times \begin{cases} 3 \sim 5 & \text{for white noise} \\ 7 \sim 10 & \text{for scale invariant} \end{cases} \quad (25)$$

where the pressure p equal σH at $t = t_{\text{eq}}$.

The reason why the combination $\bar{\mathcal{A}}_2\epsilon$ appears can be understood as follows. To describe the time evolution of r_V , we consider a simple model of the network structure. Here we consider a two-dimensional model, but the same argument can be made in three dimensions. In the following, all lengths and areas are defined in comoving coordinates, and conformal

time is used. Let $\ell_{\text{DW}}^{(\text{total})}$ be the ensemble average of the total length of the domain walls in the box of size L_{box}^2 . They are related to the area parameter \mathcal{A}_2 as

$$\frac{\ell_{\text{DW}}^{(\text{total})}}{L_{\text{box}}^2} = \mathcal{H}\mathcal{A}_2, \quad (26)$$

where we recall that \mathcal{H} is the conformal Hubble parameter. The change in the volume fraction dr_V during the time interval $d\tau$ is caused by the motion of the domain walls, and it is estimated by

$$dr_V \simeq -\frac{\ell_{\text{DW}}^{(\text{total})} \times v d\tau}{L_{\text{box}}^2} = -\mathcal{H}\mathcal{A}_2 v d\tau, \quad (27)$$

where v is the averaged velocity of the domain wall along its normal direction toward the false vacuum, and we assume $v > 0$ and $\epsilon > 0$.⁷ In the non-relativistic regime, the velocity evolves as [61]

$$\frac{dv}{d\tau} \simeq \frac{p}{\sigma}, \quad (28)$$

where $p(\propto \epsilon)$ is given in Eq. (16), and the cosmic expansion as well as the tension force can be neglected when $p \gtrsim \sigma H$ and the Lorentz gamma factor $\gamma = \mathcal{O}(1)$. Thus, the velocity is approximately given by $v \simeq (p/\sigma)(\tau - \tau')$, where τ' is an integration constant. Therefore, the decrease of r_V depends on a combination of $\mathcal{A}_2\epsilon$. Except for very large values of ϵ , it is reasonable to assume that \mathcal{A}_2 is proportional to $\bar{\mathcal{A}}_2$. This naive argument explains why the agreement becomes better when the lifetime is plotted as a function of $\bar{\mathcal{A}}_2\epsilon$ rather than ϵ .

This finding that the domain wall lifetime depends on the area parameter is new and interesting. Intuitively, the domain wall lifetime becomes longer for the inflationary fluctuations, because there are large voids and the domain walls have to traverse a larger area before they collide and annihilate.

2. Evolution with population bias

For comparison, we study the time evolution of the false-vacuum volume fraction r_V under the population bias. To handle the population bias, we interpret V_+ (V_-) in the definition of r_V as the volume of regions with more (less) initially populated volume. Following Ref. [25],

⁷ The motion due to the tension force is locally random, so this evolution equation of r_V should hold even before the bias pressure dominates over the tension force.

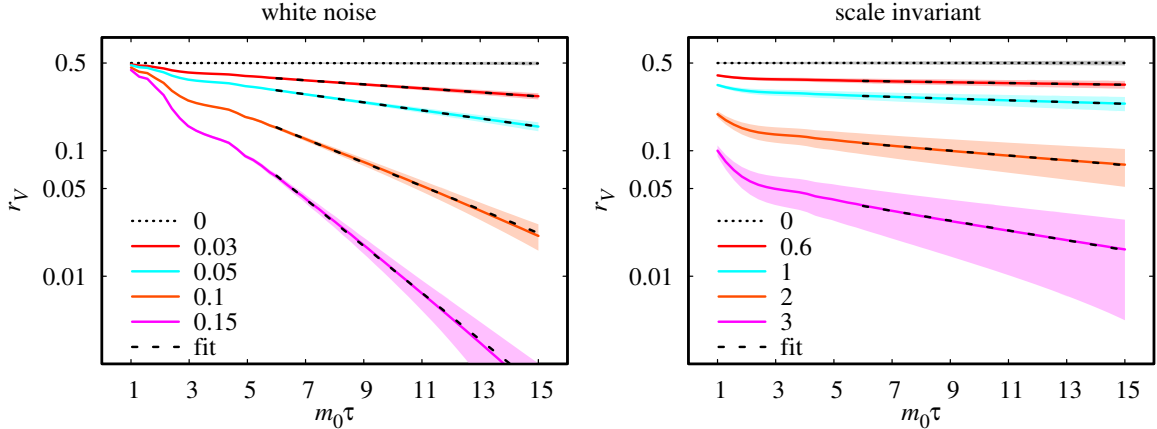


Fig. 7: Same as Fig. 5 but with the population bias, $b_d = 0 - 0.15$ for the white noise case (left) and $b_d = 0 - 3$ for the scale-invariant case (right).

we define the population bias parameter b_d as

$$b_d \equiv \begin{cases} \frac{\langle \phi \rangle}{\sqrt{\langle (\phi - \langle \phi \rangle)^2 \rangle}} & \text{for white noise fluctuations} \\ \frac{\langle \phi \rangle}{\sqrt{\mathcal{P}(k)}} & \text{for scale invariant fluctuations} \end{cases}. \quad (29)$$

Note that the variance in the denominator differs. This is to avoid the logarithmic growth of the variance in real space as a function of the box size in the case of the scale-invariant fluctuations. We also note that the relation between the initial r_V and b_d depends on the details of the distribution of ϕ . As written in Sec. IV A, our simulations choose Gaussian distributions so that both are related to the error function.

The numerical results of the time evolution of r_V are shown in Fig. 7. One can see that the domain walls are quite stable against the population bias in the case of the scale-invariant fluctuations [25]. Note that the values of b_d used for the two initial conditions are slightly different. For the numerical fit, we have used the empirical ansatz,

$$r_V \propto \exp \left[-\frac{\tau}{\tau_{\text{decay}}} \right] \quad (30)$$

which turns out to be a good fit for the numerical results. The fitting results are summarized in Table III. We find that the numerical results suggest the relation $\tau_{\text{decay}} \propto b_d^{-1.5}$.

We have also numerically estimated the average distance between domain walls across the less populated vacuum for the two initial conditions. At $\tau = 6/m_0$ it is $\sim 0.9H^{-1}$ for

white noise		scale-invariant	
b_d	$m_0\tau_{\text{decay}}$	b_d	$m_0\tau_{\text{decay}}$
0.03	27.03 ± 0.08	0.6	128.41 ± 0.98
0.05	13.54 ± 0.01	1.0	62.56 ± 0.41
0.1	4.64 ± 0.02	2.0	22.53 ± 0.14
0.15	2.32 ± 0.01	3.0	11.13 ± 0.05

Table III: Summary of τ_{decay} defined in Eq. (30) for the domain-wall network with population bias.

the white noise fluctuations with $b_d = 0.05$, while it is $\sim 2.0H^{-1}$ for the scale-invariant fluctuations with $b_d = 1$. The difference is due to the presence of large voids in the latter case. See also Fig. 1. The structure at super-horizon scales persists throughout the evolution of the domain-wall network, which explains the longevity of domain walls with inflationary initial fluctuations against the population bias.

D. Power spectrum

The power spectrum of the scalar field value and the energy density characterize the global structure of the domain-wall network. The reduced power spectrum of the energy density $\mathcal{P}_\rho(k)$ is defined as $\mathcal{P}(k)$ for ϕ (see Eq. (10)) and it satisfies

$$\langle \rho(\mathbf{x})^2 \rangle = \int d \ln k \mathcal{P}_\rho(k), \quad (31)$$

where the energy density ρ is given by

$$\rho(\mathbf{x}) = \frac{1}{2}\dot{\phi}^2 + \frac{1}{2a^2}(\nabla\phi)^2 + V(\phi). \quad (32)$$

While $\mathcal{P}(k)$ is important for the cosmic birefringence if ϕ is coupled to the Chern-Simons term of photons, $\mathcal{P}_\rho(k)$ is relevant for the curvature perturbation and the gravitational waves.

In Fig. 8 and 9 we present the numerical results on the power spectra for the white noise and scale-invariant initial fluctuations, respectively. In the upper left panel of Fig. 8 we can see that the power spectrum of the field value $\mathcal{P}(k)$ peaks at the Hubble horizon scale, $k/k_{\mathcal{H}} = 1$, and falls off sharply at scales smaller than the wall width, $k/k_{\mathcal{H}} = m_0^2\tau^2/2\pi$. Here $k_{\mathcal{H}} \equiv 2\pi\mathcal{H}$ is the comoving wavenumber corresponding to the Hubble radius. This is

in agreement with the scaling solution. On the other hand, in the upper right panel with a relatively large potential bias, the power spectrum decreases with time, implying that the domain-wall network is decaying due to the potential bias. In the lower panels, we can see that the energy power spectrum also decays with time. In particular, we can see a slight enhancement at small scales when the potential bias is large. This is probably because the ϕ particles are produced by domain wall annihilation and they generate higher momentum modes by scattering.

In the case of the inflationary initial fluctuations, the power spectrum $\mathcal{P}(k)$ becomes similarly suppressed with time, especially when there is large potential bias (see the upper right panel of Fig. 9). This is because the domains of true vacua dominate over the entire box volume, so the correlation function is strongly suppressed. On the other hand, \mathcal{P}_ρ seems to approach a scale-invariant spectrum on the large scale at late time. This is very different from the white noise case. The scale invariance of the energy density can be understood as follows. When Eq. (22) is satisfied, the domain walls begin to annihilate due to the potential bias. Around this time, the power spectrum of the false vacuum energy is approximately proportional to $\mathcal{P}(k)$, since the energy density contrast due to the false vacuum energy is proportional to ϕ . After this time, the domain-wall network mostly decays in several Hubble times (see Eq. (25)). The energy of the false vacuum is predominantly transferred to that of the ϕ particles during the decay of the domain-wall network. As a consequence, the resulting particle energy density at the end also has the scale-invariant power spectrum at the superhorizon scales, following the false vacuum power spectrum at the beginning. As we will discuss in the last section, the nearly scale-invariant energy density prevents ϕ from being the dominant dark matter, and it could also lead to probes of the scenario.

V. GRAVITATIONAL WAVES

Domain walls continue to collide and annihilate in the scaling regime, producing gravitational waves (GWs). Here we present our numerical estimates of GWs from domain walls with the two different initial fluctuations.

The amount of GWs produced by domain walls has been studied in Refs. [44–51]. In particular, the GWs produced during the collapse due to the potential bias were calculated for the first time by Murai and the present authors in Ref. [51], by considering a temperature-

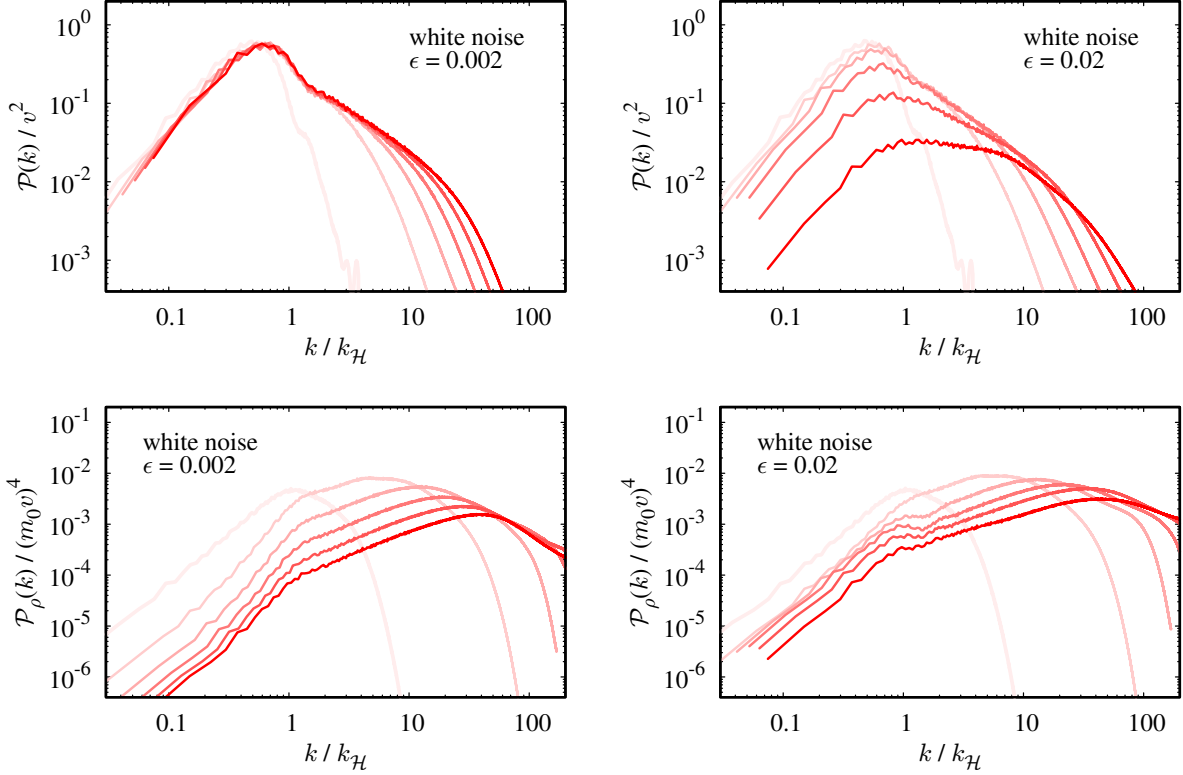


Fig. 8: The time evolution of the power spectrum of the field value (top) and energy density (bottom) for the white noise case with $\epsilon = 0.002$ (left) and 0.02 (right). The color of the lines indicates the temporal evolution of the results, with darker colors representing later times (equally spaced between $\tau = 6 - 20/m_0$).

dependent bias. Before that, most of the works used the GWs estimated in Ref. [46] where they did not include the potential bias term in the numerical lattice calculations. The omission of the bias term was primarily due to the extended lifetime of the domain-wall network under a bias that ensures the system achieves a scaling solution well before annihilation. Additionally, accurately simulating the annihilation process within the constraints of numerical simulation time posed significant challenges. Here our focus is on the difference between the white noise and scale-invariant initial fluctuations, so we estimate the GWs during the scaling regime without introducing the potential bias term, following the spirit of Ref. [46]. The GW spectrum after the domain wall collapse can be approximately estimated by evaluating

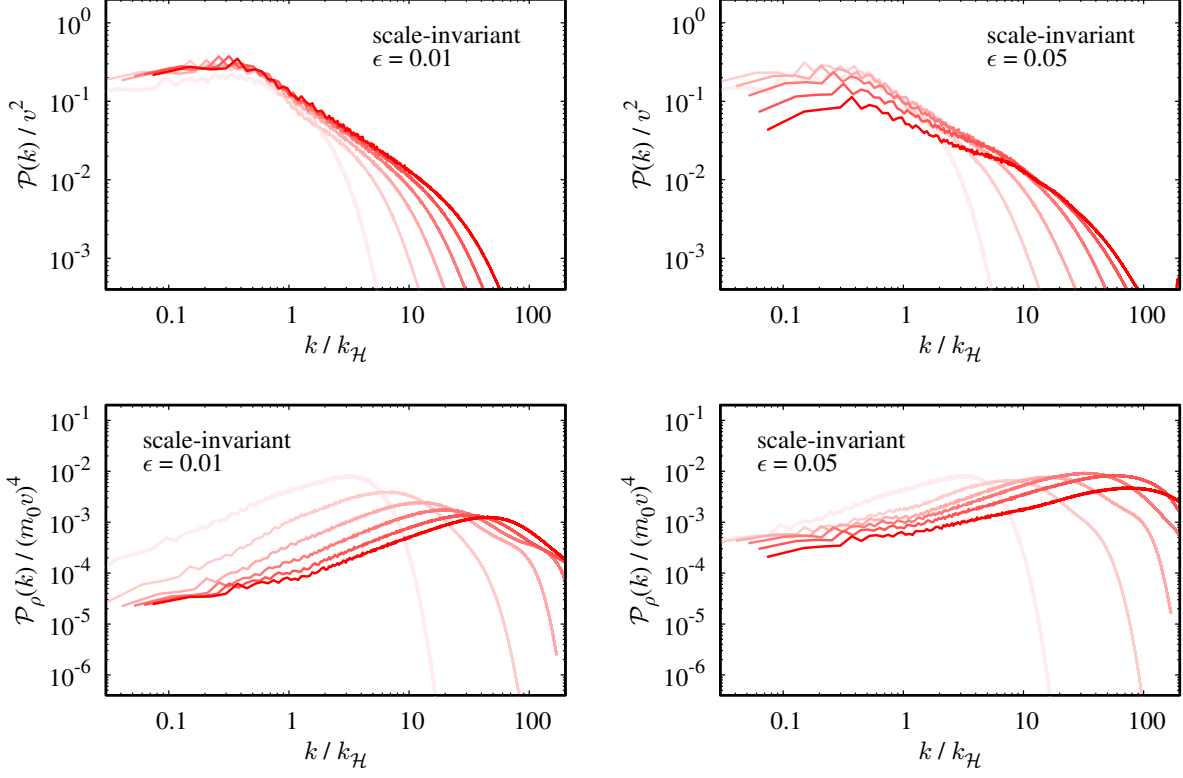


Fig. 9: Same as Fig. 8 but for the scale-invariant case with $\epsilon = 0.01$ (left) and 0.05 (right).

the GW in the scaling regime at the time of the decay, determined by Eq. (22).⁸ We leave it to future work to estimate the GWs emitted during the collapse for the inflationary initial fluctuations.

The tensor perturbation of the metric in a spatially flat FLRW universe is given by

$$ds^2 = -dt^2 + a^2(t)(\delta_{ij} + h_{ij})dx^i dx^j, \quad (33)$$

where h_{ij} is the transverse and traceless tensor with $|h_{ij}| \ll 1$. The equation of motion for h_{ij} is

$$\ddot{h}_{ij} + 3H\dot{h}_{ij} - \frac{1}{a^2}\Delta h_{ij} = \frac{2}{M_{\text{pl}}^2}\Lambda_{ij}{}^{kl}T_{kl}, \quad (34)$$

where M_{pl} is the reduced Planck mass, T_{ij} is a stress tensor, and $\Lambda_{ij}{}^{kl}$ is a projection onto the transverse and traceless components of the stress tensor. In our scenario we use the stress tensor for the scalar field.

⁸ Note, however, that the main production of the GWs occurs during the collapse of domain walls [51].

The GW spectrum is estimated as

$$\Omega_{\text{GW}}(k, t) = \frac{1}{\rho_c(t)} \rho_{\text{GW}}(k, t) \quad (35)$$

$$\rho_{\text{GW}}(k, t) \equiv \frac{M_{\text{pl}}^2}{4} \left\langle \dot{h}_{ij}(k, t) \dot{h}_{ij}(k, t) \right\rangle, \quad (36)$$

where $\Omega_{\text{GW}}(k, t)$ and $\rho_{\text{GW}}(k, t)$ are the density parameter and the energy density of GWs per the unit logarithmic wavenumber, respectively, $\rho_c(t) = 3H^2 M_{\text{pl}}^2$ is the critical density at time t , and the bracket represents the spatial average. Let us introduce the so-called efficiency parameter ϵ_{GW} [46],

$$\rho_{\text{GW}}(k, t) = \frac{\epsilon_{\text{GW}}(k, t) \mathcal{A}_3^2 \sigma^2}{32\pi M_{\text{pl}}^2}, \quad (37)$$

where ϵ_{GW} should be of order unity around the peak frequency in the scaling regime, and \mathcal{A}_3 is the area parameter in the absence of any biases.

In the scaling regime, the typical distance between domain walls is of order the Hubble radius. The GW spectrum has a peak at the corresponding scale,

$$k_{\text{peak}} \sim k_{\mathcal{H}} = 2\pi aH \quad (38)$$

with the GW density parameter,

$$\Omega_{\text{GW}}(k_{\text{peak}}, t) = \frac{\tilde{\epsilon}_{\text{GW}} \mathcal{A}_3^2 \sigma^2}{96\pi M_{\text{pl}}^4 H^2}, \quad (39)$$

where $\tilde{\epsilon}_{\text{GW}}(t) \equiv \epsilon_{\text{GW}}(k_{\text{peak}}, t)$, and it was estimated to be $\tilde{\epsilon}_{\text{GW}} \simeq 0.7 \pm 0.4$ in Ref. [46]. We have seen that the value of \mathcal{A}_2 differs by a factor of 2 between the white noise and scale-invariant fluctuations in the case of the two-dimensional simulations. See the line of $\epsilon = 0$ in Fig. 4. We have confirmed that this is also the case for the three-dimensional case. See Fig. 10. We can see that the evolution of \mathcal{A}_3 is very similar to that of \mathcal{A}_2 . Therefore, the peak frequency for the scale-invariant fluctuations is expected to be lower by a factor of about two than for the white noise fluctuations.

We have performed numerical simulations on a three-dimensional lattice with $N_{\text{grid}} = 1024$. The box contains $\sim 50^3$ Hubble horizons at the initial time $\tau_i = 1/m_0$. As we mentioned, we do not introduce potential biases, setting $\epsilon = 0$. The simulation is stopped at a time $\tau_{\text{end}} = 20/m_0$. In Fig. 11 we show the GW spectra obtained by averaging the results of 15 simulations. These simulations were performed with the white noise (left) and

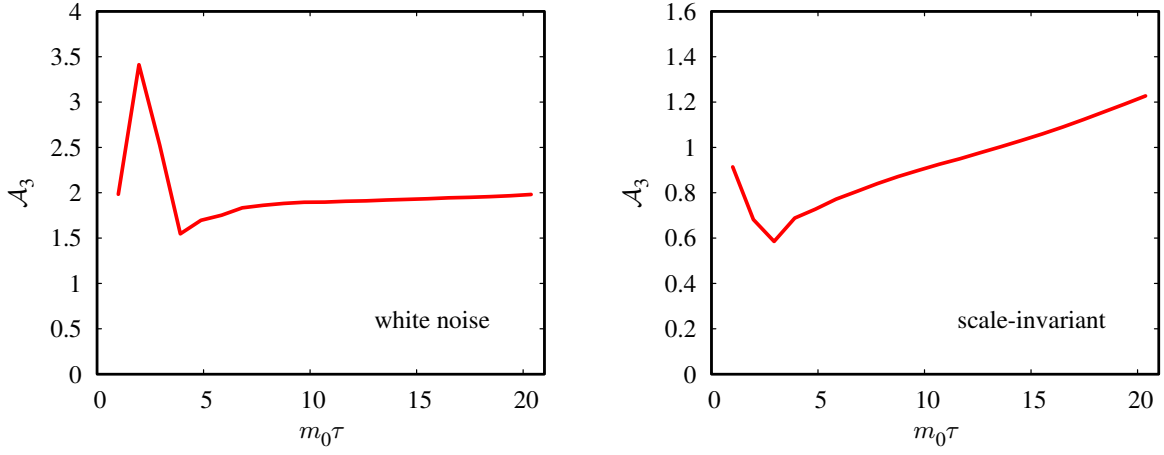


Fig. 10: The time evolution of \mathcal{A}_3 without any biases for the white noise (left) and scale-invariant (right).

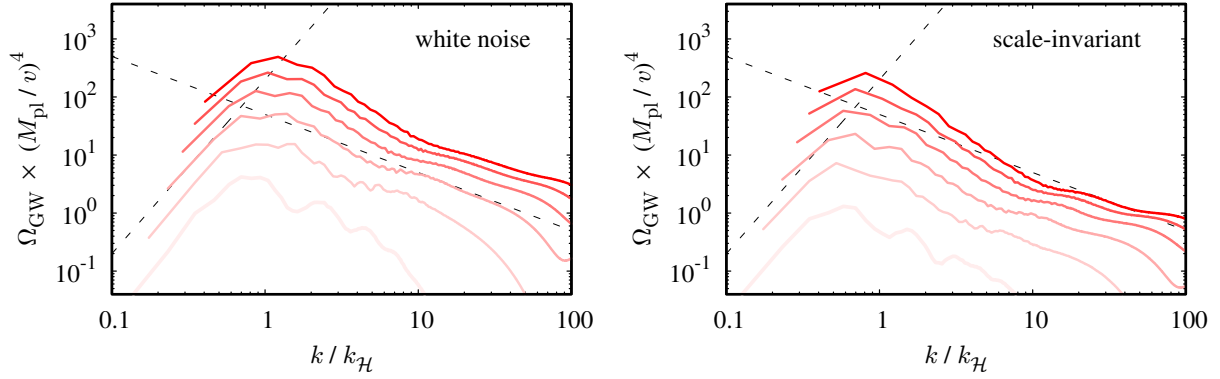


Fig. 11: GW spectra from 15 realizations for the white noise (left) and scale-invariant (right) cases, with no potential bias. The color of the lines indicates the time evolution within $\tau = 6/m_0 - 20/m_0$, with darker colors corresponding to later times. Black dashed lines represent power laws $\propto k^3$ and $\propto k^{-1}$, respectively, to guide the eye.

the scale-invariant (right) initial fluctuations. The color of the lines represents the time evolution, with darker colors corresponding to data at later times. Specifically, we show the data at $\tau \simeq 6, 9, 12, 15, 17$, and $20/m_0$.

The comparison of the GW spectra for both cases shows a similarity in the overall shapes. This should be contrasted with the power spectra of the energy density, which are clearly

different at large scales. This implies that the energy density distribution at superhorizon scales does not lead to the production of GWs, which is consistent with our intuition.

Looking more closely at the spectrum, both spectra show the same power-law behavior at large scales ($\propto k^3$) and small scales ($\propto k^{-1}$), respectively. This wavenumber dependence agrees with the finding of Ref. [46] which adopted the initial fluctuations of a massless scalar field in the Minkowski space. However, we can see that the peak shifts toward lower frequencies, resulting in reduced GWs for the scale-invariant case. The difference can be attributed to the difference of \mathcal{A}_3 . The peak frequency corresponds to the typical correlation length of the domain-wall network, and the GW emission depends on the total energy stored in the network as well as the curvature radius of domain walls.

In Fig. 12, we show the spectrum of the efficiency parameter with respect to the wavenumber rescaled by $\mathcal{A}_3 k_{\mathcal{H}}$, which corresponds to the typical distance scale between domain walls. Note that we take account of the time-dependence of \mathcal{A}_3 . We can see that at any given time, the spectrum around the peak frequency behaves almost the same without much dependence on the two initial conditions. Choosing the data at $\tau = \tau_{\text{end}}$, our results show $\tilde{\epsilon}_{\text{GW}}$ to be

$$\tilde{\epsilon}_{\text{GW}} = \begin{cases} 0.25 \pm 0.04 & \text{for white noise} \\ 0.34 \pm 0.14 & \text{for scale invariant} \end{cases}, \quad (40)$$

where the errors come from variations of Ω_{GW} and \mathcal{A}_3 across realizations. These values are smaller than those of Ref. [46]. However, considering the difference in the method of evaluating the area parameter as well as the initial condition, it is not straightforward to compare our results with theirs. While we use the white noise initial fluctuations, Ref. [46] adopted fluctuations of a massless scalar field in the Minkowski space. Apart from the different initial conditions, our method tends to count the area of walls more than the reference. Specifically, Ref. [46] gives $\mathcal{A} \simeq 0.8 \pm 0.1$, which would imply $\mathcal{A}_3 \simeq 1.6 \pm 0.2$ in the non-relativistic approximation. On the other hand, we have $\mathcal{A}_3 \simeq 2$ for the white noise fluctuations, which makes our estimate of $\tilde{\epsilon}_{\text{GW}}$ smaller by a factor of 1.6. Given this difference in the estimate of the area parameter, our result for the white noise fluctuations is consistent with Ref. [46], although such a direct comparison may not be justified since different initial conditions are used. Therefore, our results show that by considering the dependence of the peak height and peak frequency of the GW spectrum on the area parameter, we can predict the gravitational wave spectrum independently of the time and nature of the initial

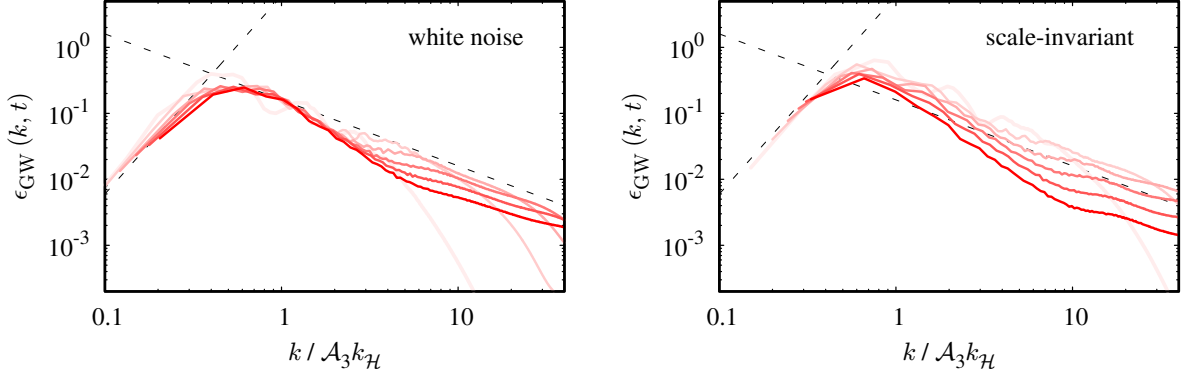


Fig. 12: Same as Fig. 11 but the horizontal axis is re-scaled by $\mathcal{A}_3(\tau)$ and the vertical axis is the efficiency parameter $\epsilon_{\text{GW}}(k, t)$.

fluctuations. In particular, based on our results, we improve the estimate of the peak wavenumber given by Eq. (38) as follows

$$k_{\text{peak}} \simeq \mathcal{A}_3 k_{\mathcal{H}} = 2\pi a \mathcal{A}_3 H, \quad (41)$$

under the scaling regime. The peak wavenumber (41) takes into account the area parameter dependence, which reflects the global structure of the domain-wall network. Note, however, that if \mathcal{A}_3 is much less than unity, e.g. due to dilution by secondary inflation, we expect this relationship to break down due to the limitation of causality.

VI. DISCUSSION AND CONCLUSIONS

In this paper we have studied the evolution of the domain-wall network in the presence of the potential and population biases for the two different initial fluctuations, thermal and inflationary fluctuations. In particular, this is the first to study the domain-wall network with the inflationary fluctuations under the influence of the potential bias. While in our previous work the domain-wall network was found to be very robust against the population bias for the inflationary fluctuations, we find that the domain walls decay under the potential bias with a lifetime several times longer than for the thermal fluctuations. Importantly, we have found that this difference of the lifetime arises from the area parameter since it determines the averaged distance between domain walls. This dependence on the area parameter has been overlooked in the literature, which has focused only on thermal initial fluctuations.

This led us to derive a improved formula for the domain wall lifetime. One of the important lessons we have learned in this work is that the choice of initial fluctuations is important for the evolution of domain walls.

We have estimated the gravitational waves generated by domain wall annihilation for both types of initial fluctuations. The resulting gravitational wave spectrum has a peak frequency around the Hubble horizon at the time of annihilation, but the peak location is different due to the different lifetimes for the two types of initial fluctuations. We have shown that the gravitational wave spectrum can be understood in a unified manner by taking account of the dependence of the peak height and frequency of the spectrum on the area parameter.

One important application of our results is the axion domain walls coupled to photons, which can naturally explain the isotropic cosmic birefringence [37] recently suggested by analyses in Refs.[56, 57, 62]. A crucial assumption is the absence of cosmic strings attached to these domain walls. If cosmic strings were present, anisotropic cosmic birefringence would likely dominate, making it challenging to account for the observed isotropic cosmic birefringence as discussed in Refs. [37, 63]. As discussed in the Appendix, such axion domain walls can form naturally from the inflationary fluctuations that the axion acquired during inflation. While there is an inherent population bias, the axion domain walls are stable against the population bias [25].⁹ However, they might still be subject to potential bias if the axion potential receives additional contributions. To explain the isotropic cosmic birefringence, the potential bias must be sufficiently small so that the axion domain walls exist until the time of recombination. In particular, the pressure due to the potential bias should be smaller than σH_{rec} , where $H_{\text{rec}} \simeq 3 \times 10^{-29}$ eV is the Hubble parameter at the time of recombination. This implies that the potential energy difference between the true and false vacua must be smaller than the product of the height of the axion potential and the ratio of the Hubble parameter at recombination to the axion mass.

We have primarily considered domain wall collapses under the influence of biases. After the collapse of the domain wall, most of the energy is converted into ϕ particles. These

⁹ Note that it is the population bias defined on the last scattering surface, b_d^{LSS} , that is relevant for isotropic cosmic birefringence, while it is generally different from b_d defined in the three-dimensional universe (see Eq. (29)) due to the stochastic nature of the domain walls. However, for $b_d \lesssim \mathcal{O}(1)$, which is required for the stability of the axion domain walls, b_d^{LSS} is also expected to satisfy $b_d^{\text{LSS}} \lesssim \mathcal{O}(1)$. This population bias implies an uncertainty in the predicted rotation angle, but still favors the axion-photon anomaly coefficient of $\mathcal{O}(1)$ to explain the observed cosmic birefringence.

particles soon become non-relativistic and may contribute to dark matter. In fact, we have numerically confirmed that the total energy density does indeed scale as nonrelativistic matter after the domain walls have largely collapsed. Such nonthermal production of dark matter can be an important production mechanism, especially when the particles are light. Therefore, our study has important implications for the production of dark matter by domain wall collapse. However, one must pay attention to the initial fluctuations. This is because, if the domain wall originates from the inflationary fluctuations, the resulting particle energy density is expected to have a scale-invariant power spectrum at large scales (see Fig. 9). This contributes to the isocurvature perturbations with large non-Gaussianity, which would be inconsistent with observations if it were a significant fraction of dark matter. A similar argument implies that if the domain wall originates from the inflationary fluctuations, the energy density of the domain wall must be much smaller than the other components when it decays, since otherwise it would generate too large curvature perturbations with sizable non-Gaussianity.¹⁰ Thus, the cosmological domain wall problem is more severe for the domain walls from the inflationary initial fluctuations. From another point of view, the isocurvature perturbations with significant non-Gaussianity could be a probe of the domain walls from the inflationary fluctuations. In particular, axion domain walls can be formed naturally by inflationary fluctuations in string theory, which contains many axions. Thus, the axion domain wall and its observational implications might be used to probe the string theory.

Acknowledgments

This work is supported by JSPS Core-to-Core Program (grant number: JPJSCCA20200002) (J.L. and F.T.), JSPS KAKENHI Grant Numbers 19H01894 (N.K.), 20H01894 (F.T. and N.K.), 20H05851 (F.T., N.K. and W.Y.), 21H01078 (N.K.), 21K20364 (W.Y.), 22K14029 (W.Y.), 22H01215 (W.Y.), Graduate Program on Physics for the Universe (J.L.), and Watanuki International Scholarship Foundation (J.L.). This article is based upon work from COST Action COSMIC WISPerS CA21106, supported by COST (European Cooperation in Science and Technology).

¹⁰ Therefore, the GWs from axion domain walls with initial inflationary fluctuations are unable to explain the NANOGrav results [52]. See also Refs. [47, 50, 51].

Appendix A: Phase transition with inflationary fluctuations

We introduce a novel mechanism for domain wall/string formation that is similar to the Kibble mechanism [2]. Instead of utilizing the thermal potential to establish a symmetric phase, we exploit the effects of the stochastic dynamics, allowing the presence of a non-minimal coupling. As we will see, this mechanism leads to phenomena that differ significantly from the Kibble mechanism and naturally result in the formation of topological defects through inflationary fluctuations. A similar mechanism was mentioned in Ref. [64] in the context of string/texture formation and in Ref. [28] with a time-dependent Hubble parameter during inflation. However, this study examines domain-wall network formation using a Hubble-induced mass with an almost constant Hubble parameter during inflation, which has never been explored before. Since the non-minimal coupling will be generated radiatively, it is natural to take it into account. This non-minimal coupling and stochastic dynamics make domain wall formation by inflationary fluctuations a very plausible scenario. In the case of the axion domain wall, we examine the parameter range in which strings do not form. This allows for an explanation of isotropic cosmic birefringence [37].

The details of the phase transition depend on the UV completion of the models, so in the following we consider the Z_2 model and the axion separately.

1. Case of Z_2 domain wall

Here we present a simple model similar to the usual domain wall formation associated with a phase transition. We expect analogous domain wall formation in a larger class of models. We consider a non-minimal coupling

$$\mathcal{L} = -c_H \frac{\phi^2 R}{2} \tag{A1}$$

with $c_H > 0$, where R is the Ricci scalar given by $R = 6(\dot{a}/a + (\dot{a}/a)^2)$ in the flat FLRW universe. We note that a very small non-minimal coupling is unnatural if ϕ has interaction because it is generated radiatively. During inflation, the field ϕ acquires a positive Hubble-induced mass squared,

$$m_{\text{Hubble}}^2 = 6c_H H_{\text{inf}}^2, \tag{A2}$$

where H_{inf} is the Hubble parameter during the inflationary period as in the main part. With the quartic coupling or other interactions, we also have a “thermal” mass squared of $\mathcal{O}(\lambda)H_{\text{inf}}^2$

induced by the Gibbons-Hawking radiation. We include such additional contribution(s) by redefining c_H and call the two contributions Hubble-induced mass. In the following, we assume $m_{\text{Hubble}}^2 > m_0^2$ so that the effective potential is minimized at $\phi = 0$. Then the system is similar to the usual Kibble mechanism where the SSB is induced by the time evolution of the thermal potential. The only difference is that the system is lifted into the symmetric vacuum by the Hubble-induced mass, but not by the real thermal mass. Below, we consider two cases with respect to the magnitude of c_H .

a. $c_H \gtrsim (0.1)$ In the case $c_H \gtrsim (0.1)$, we have the positive m_{Hubble}^2 mass larger than H_{inf}^2 , and thus the inflationary fluctuation is suppressed at superhorizon scales. After the inflation, the Hubble parameter H starts to decrease. When the time-dependent effective mass determined by the sum of m_{Hubble}^2 and $V''(\phi)$ becomes comparable to H , the Z_2 symmetry gets spontaneously broken and the domain walls are formed with white noise fluctuation.

b. $c_H \lesssim 0.1$ This case is our primary focus. Note that we still assume that $m_{\text{Hubble}}^2 \gg m_0^2$, and thus, we have a symmetric phase of ϕ during inflation. However,

$$m_{\text{Hubble}}^2 \lesssim H_{\text{inf}}^2, \quad (\text{A3})$$

implies that inflationary fluctuations of ϕ are not suppressed at superhorizon scales, and thus ϕ in each Hubble horizon diffuses like the random walk during inflation. The diffusion due to the random walk leads to the growth of the variance, $\phi^2 \sim tH_{\text{inf}}^3/(2\pi)^2$, which is balanced by the classical motion due to the mass term, $m_{\text{Hubble}}^2\phi^2/2$. If the inflation lasts long enough, we obtain the equilibrium distribution with the probability [60, 65–71]¹¹

$$P[\phi] \propto \exp\left\{-\frac{8\pi^2}{3H_{\text{inf}}^4}\left(V(\phi) + \frac{m_{\text{Hubble}}^2\phi^2}{2}\right)\right\}. \quad (\text{A4})$$

This is a probability distribution ϕ in a single Hubble patch during inflation. By neglecting the contribution of V , this distribution is reached with a time scale

$$N_{\text{eq}} \sim \frac{H_{\text{inf}}^2}{m_{\text{Hubble}}^2} \sim \frac{1}{6c_H}. \quad (\text{A5})$$

The scalar potential $V(\phi)$, especially the quartic coupling, could reduce the amount of e-folds required to reach the equilibrium.¹² If N_{eq} is much smaller than the e-folds for the

¹¹ This stochastic distribution of scalar field was discussed in the context of the axion dark matter [60, 68, 69, 71–73] (without the non-minimal coupling), relaxion [74], and scalar/vector boson dark matter with the non-minimal coupling [70].

¹² As discussed in the main text, the initial fluctuations for domain walls transition from inflationary to thermal in this case.

observable Universe, N , ϕ in the whole observable Universe follows this distribution, i.e. the population bias is close to zero if $N \gg N_{\text{eq}}$. This is the case with

$$c_H = \mathcal{O}(0.001 - 0.1). \quad (\text{A6})$$

The effect of the finite mass slightly deviates the power spectrum of the initial fluctuations from the scale-invariance, but our conclusions do not change.

The above discussion shows that unless $c_H(> 0)$ is much smaller than unity (i.e. $c_H < 10^{-3}$), domain walls are naturally formed with either the initial condition of white noise or scale-invariant fluctuations depending on the size of c_H .

2. Case of axionic domain walls

Next, we consider the axionic domain wall formation. As a UV theory, we consider a model with an approximate global U(1) symmetry. The potential is given similarly as

$$V = -m_0^2 |\Phi|^2 + \frac{\lambda}{4} |\Phi|^4 \quad (\text{A7})$$

where the potential minimum is

$$\langle |\Phi| \rangle = \sqrt{\frac{m_0^2}{2\lambda}} \equiv \frac{f_a}{\sqrt{2}} \quad (\text{A8})$$

and a Nambu-Goldstone boson or axion, a , appears in the phase,

$$\Phi = \left(\frac{f_a}{\sqrt{2}} + s \right) e^{ia/f_a}. \quad (\text{A9})$$

Here s is the radial mode. The axion acquires a potential via the explicit breaking of the U(1) symmetry, such as $\delta V \propto \text{Re } \Phi$.

Again let us consider a non-minimal coupling

$$\mathcal{L} = -c_H |\Phi|^2 R, \quad (\text{A10})$$

and the resultant Hubble-induced mass

$$m_{\text{Hubble}}^2 = 6c_H H_{\text{inf}}^2, \quad (\text{A11})$$

for the Φ field. Let us consider again the effect of this term by neglecting the bare potential of Φ during the inflation.

a. $c_H \gtrsim 0.1$ We have the symmetry restoration during inflation. Since Φ is heavy, the inflationary fluctuation is suppressed. After the inflation, when the tachyonic mass $-m_0^2$ takes over the Hubble-induced mass, the U(1) symmetry gets spontaneously broken. We obtain the usual string-wall network. This system has an initial fluctuation approximated by the white noise for Φ .

b. $0 \lesssim c_H \lesssim 0.1$ In this case, we have the equilibrium distribution of the two fields,

$$P[\text{Re } \Phi, \text{Im } \Phi] \propto \exp\left\{-\frac{8\pi^2}{3H_{\text{inf}}^4} \left(V + \frac{m_{\text{Hubble}}^2((\text{Re } \Phi)^2 + (\text{Im } \Phi)^2)}{2}\right)\right\}. \quad (\text{A12})$$

We have a flat distribution for the axion $\propto \arg \Phi$ by neglecting the axion mass (The inflationary dynamics rarely change the axion potential because of the U(1) symmetry). Again, we obtain the field configuration leading to the formation of strings if $N > N_{\text{eq}} \sim 1/(6c_H)$. However, this follows the string-wall network from inflationary fluctuation, which is not our focus.¹³

We, therefore, need to consider

$$N \lesssim N_{\text{eq}} \sim 1/(6c_H). \quad (\text{A13})$$

In this case, we expand $\Phi = \bar{\Phi} + \delta\Phi$, where $\bar{\Phi}$ follows the equilibrium distribution. By neglecting the mass effect, the $\delta\Phi$ distribution from the random jump forms a disk with a radius

$$\sqrt{N} \frac{H_{\text{inf}}}{2\pi} \sim \sqrt{6c_H N} |\bar{\Phi}| / \xi. \quad (\text{A14})$$

Here we have introduced ξ to characterize the tuning from the typical value of $\bar{\Phi}$, the 1σ deviation of the probability distribution, $|\bar{\Phi}| = \xi \sqrt{\frac{3H_{\text{inf}}^4}{4\pi^2 m_{\text{Hubble}}^2}}$. If $c_H \sim \mathcal{O}(0.001)$, the domain wall without string can be formed with $\mathcal{O}(10\%)$ tuning, because the symmetric point cannot be covered by the disk with $\xi = \mathcal{O}(1)$, while the axion potential hilltop can be covered at a probability of $2N_{\text{DW}} \times \sqrt{N} \frac{H_{\text{inf}}}{2\pi} / (2\pi\bar{\Phi})$ with N_{DW} being the domain wall number.

c. $c_H \lesssim 0$ A much simpler scenario is the case of the negative Hubble-induced mass[37]. If the Φ has a negative mass-squared, it is driven to the non-zero expectation value,

$$|\Phi| \sim \sqrt{2|m_{\text{Hubble}}|^2/\lambda} \quad (\text{A15})$$

¹³ We can avoid the string formation if we introduce a sufficiently large explicit breaking term of U(1) in non-minimal coupling, $\Phi^2 R^2$. We also point out it is important to take account of the long-range correlation when we discuss the string-wall network from the inflationary fluctuation. Our lattice simulation shows a longer lifetime against the population bias than the white noise case, and larger string loops, which can give interesting gravitational wave spectra.

induced by the Hubble-induced mass. Here, we include the quartic coupling but neglect the m_0^2 term. This is of $\mathcal{O}(H_{\text{inf}})$ if

$$\lambda \sim |c_H|. \quad (\text{A16})$$

Then it is very natural to have the domain wall formation without strings because the random jump of the axion $a \sim \sqrt{N}H_{\text{inf}}/2\pi$ is around the effective decay constant $f_{\text{eff}} \simeq |\Phi| \sim H_{\text{inf}}$. If $|c_H|$ is greater than or around unity, the radial direction becomes heavier than H_{inf} , and the fluctuation in the radial direction can be neglected. Even if this is not the case, the string formation is disfavored by the field probability distribution. After inflation, we need to keep Φ in the broken phase. To this end, we can consider the interaction of negative thermal mass squared through the portal coupling between Φ and the Standard Model Higgs field.

-
- [1] Y. B. Zeldovich, I. Y. Kobzarev, and L. B. Okun, *Zh. Eksp. Teor. Fiz.* **67**, 3 (1974).
 - [2] T. W. B. Kibble, *J. Phys. A* **9**, 1387 (1976).
 - [3] A. Vilenkin, *Phys. Rev. D* **23**, 852 (1981).
 - [4] A. Vilenkin and E. P. S. Shellard, *Cosmic Strings and Other Topological Defects* (Cambridge University Press, 2000), ISBN 978-0-521-65476-0.
 - [5] W. H. Press, B. S. Ryden, and D. N. Spergel, *Astrophys. J.* **347**, 590 (1989).
 - [6] M. Hindmarsh, *Phys. Rev. Lett.* **77**, 4495 (1996), hep-ph/9605332.
 - [7] T. Garagounis and M. Hindmarsh, *Phys. Rev. D* **68**, 103506 (2003), hep-ph/0212359.
 - [8] J. C. R. E. Oliveira, C. J. A. P. Martins, and P. P. Avelino, *Phys. Rev. D* **71**, 083509 (2005), hep-ph/0410356.
 - [9] P. P. Avelino, C. J. A. P. Martins, and J. C. R. E. Oliveira, *Phys. Rev. D* **72**, 083506 (2005), hep-ph/0507272.
 - [10] A. M. M. Leite and C. J. A. P. Martins, *Phys. Rev. D* **84**, 103523 (2011), 1110.3486.
 - [11] A. M. M. Leite, C. J. A. P. Martins, and E. P. S. Shellard, *Phys. Lett. B* **718**, 740 (2013), 1206.6043.
 - [12] C. J. A. P. Martins, I. Y. Rybak, A. Avgoustidis, and E. P. S. Shellard, *Phys. Rev. D* **93**, 043534 (2016), 1602.01322.
 - [13] A. Vilenkin, *Phys. Rept.* **121**, 263 (1985).
 - [14] G. B. Gelmini, M. Gleiser, and E. W. Kolb, *Phys. Rev. D* **39**, 1558 (1989).

- [15] S. E. Larsson, S. Sarkar, and P. L. White, Phys. Rev. D **55**, 5129 (1997), hep-ph/9608319.
- [16] Z. Lalak, S. Lola, and P. Magnowski, Phys. Rev. D **78**, 085020 (2008), 0710.1233.
- [17] J. R. C. C. C. Correia, I. S. C. R. Leite, and C. J. A. P. Martins, Phys. Rev. D **90**, 023521 (2014), 1407.3905.
- [18] J. R. C. C. C. Correia, I. S. C. R. Leite, and C. J. A. P. Martins, Phys. Rev. D **97**, 083521 (2018), 1804.10761.
- [19] Z. Lalak and S. Thomas, Phys. Lett. B **306**, 10 (1993), hep-ph/9303250.
- [20] Z. Lalak, B. A. Ovrut, and S. Thomas, Phys. Rev. D **51**, 5456 (1995).
- [21] Z. Lalak, S. Lola, B. A. Ovrut, and G. G. Ross, Nucl. Phys. B **434**, 675 (1995), hep-ph/9404218.
- [22] D. Coulson, Z. Lalak, and B. A. Ovrut, in PASCOS / HOPKINS 1995 (1995), pp. 429–444, hep-ph/9508226.
- [23] D. Coulson, Z. Lalak, and B. A. Ovrut, Phys. Rev. D **53**, 4237 (1996).
- [24] T. Krajewski, J. H. Kwapisz, Z. Lalak, and M. Lewicki, Phys. Rev. D **104**, 123522 (2021), 2103.03225.
- [25] D. Gonzalez, N. Kitajima, F. Takahashi, and W. Yin, Phys. Lett. B **843**, 137990 (2023), 2211.06849.
- [26] A. D. Linde and D. H. Lyth, Phys. Lett. B **246**, 353 (1990).
- [27] D. H. Lyth, Phys. Rev. D **45**, 3394 (1992).
- [28] M. Nagasawa and J. Yokoyama, Nucl. Phys. B **370**, 472 (1992).
- [29] M. Y. Khlopov, S. G. Rubin, and A. S. Sakharov, Astropart. Phys. **23**, 265 (2005), astro-ph/0401532.
- [30] H. Davoudiasl, S. Sarangi, and G. Shiu, Phys. Rev. Lett. **99**, 161302 (2007), hep-th/0611232.
- [31] N. Kitajima and F. Takahashi, Phys. Lett. B **745**, 112 (2015), 1502.03725.
- [32] R. Daido, N. Kitajima, and F. Takahashi, JCAP **07**, 046 (2015), 1504.07917.
- [33] R. Daido, N. Kitajima, and F. Takahashi, Phys. Rev. D **92**, 063512 (2015), 1505.07670.
- [34] T. Kobayashi and F. Takahashi, JCAP **08**, 056 (2016), 1607.04294.
- [35] J. Liu, R.-G. Cai, and Z.-K. Guo, Phys. Rev. Lett. **126**, 141303 (2021), 2010.03225.
- [36] A. S. Sakharov, Y. N. Eroshenko, and S. G. Rubin, Phys. Rev. D **104**, 043005 (2021), 2104.08750.
- [37] F. Takahashi and W. Yin, JCAP **04**, 007 (2021), 2012.11576.

- [38] N. Kitajima, F. Kozai, F. Takahashi, and W. Yin, *JCAP* **10**, 043 (2022), 2205.05083.
- [39] M. Redi and A. Tesi, *Phys. Rev. D* **107**, 095032 (2023), 2211.06421.
- [40] M. Gorghetto, E. Hardy, H. Nicolaescu, A. Notari, and M. Redi (2023), 2311.09315.
- [41] J. Preskill, S. P. Trivedi, F. Wilczek, and M. B. Wise, *Nucl. Phys. B* **363**, 207 (1991).
- [42] S. Chang, C. Hagmann, and P. Sikivie, *Phys. Rev. D* **59**, 023505 (1999), hep-ph/9807374.
- [43] M. Gleiser and R. Roberts, *Phys. Rev. Lett.* **81**, 5497 (1998), astro-ph/9807260.
- [44] T. Hiramatsu, M. Kawasaki, and K. Saikawa, *JCAP* **05**, 032 (2010), 1002.1555.
- [45] M. Kawasaki and K. Saikawa, *JCAP* **09**, 008 (2011), 1102.5628.
- [46] T. Hiramatsu, M. Kawasaki, and K. Saikawa, *JCAP* **02**, 031 (2014), 1309.5001.
- [47] T. Higaki, K. S. Jeong, N. Kitajima, T. Sekiguchi, and F. Takahashi, *JHEP* **08**, 044 (2016), 1606.05552.
- [48] K. Nakayama, F. Takahashi, and N. Yokozaki, *Phys. Lett. B* **770**, 500 (2017), 1612.08327.
- [49] K. Saikawa, *Universe* **3**, 40 (2017), 1703.02576.
- [50] R. Z. Ferreira, A. Notari, O. Pujolas, and F. Rompineve, *JCAP* **02**, 001 (2023), 2204.04228.
- [51] N. Kitajima, J. Lee, K. Murai, F. Takahashi, and W. Yin (2023), 2306.17146.
- [52] A. Afzal et al. (NANOGrav), *Astrophys. J. Lett.* **951**, L11 (2023), 2306.16219.
- [53] J. Antoniadis et al. (EPTA, InPTA:), *Astron. Astrophys.* **678**, A50 (2023), 2306.16214.
- [54] D. J. Reardon et al., *Astrophys. J. Lett.* **951**, L6 (2023), 2306.16215.
- [55] H. Xu et al., *Res. Astron. Astrophys.* **23**, 075024 (2023), 2306.16216.
- [56] Y. Minami and E. Komatsu, *Phys. Rev. Lett.* **125**, 221301 (2020), 2011.11254.
- [57] P. Diego-Palazuelos et al., *Phys. Rev. Lett.* **128**, 091302 (2022), 2201.07682.
- [58] D. Gonzalez, Ph.D. thesis, Tohoku University (2023).
- [59] M. Kawasaki, K. Saikawa, and T. Sekiguchi, *Phys. Rev. D* **91**, 065014 (2015), 1412.0789.
- [60] K. Murai, F. Takahashi, and W. Yin, *Phys. Rev. D* **108**, 036020 (2023), 2305.18677.
- [61] P. P. Avelino, C. J. A. P. Martins, and L. Sousa, *Phys. Rev. D* **78**, 043521 (2008), 0805.4013.
- [62] J. R. Eskilt (2022), 2201.13347.
- [63] M. Jain, A. J. Long, and M. A. Amin, *JCAP* **05**, 055 (2021), 2103.10962.
- [64] H. M. Hodges and J. R. Primack, *Phys. Rev. D* **43**, 3155 (1991).
- [65] A. A. Starobinsky, *Lect. Notes Phys.* **246**, 107 (1986).
- [66] A. A. Starobinsky and J. Yokoyama, *Phys. Rev. D* **50**, 6357 (1994), astro-ph/9407016.
- [67] R. J. Hardwick, V. Vennin, C. T. Byrnes, J. Torrado, and D. Wands, *JCAP* **10**, 018 (2017),

1701.06473.

- [68] P. W. Graham and A. Scherlis, *Phys. Rev. D* **98**, 035017 (2018), 1805.07362.
- [69] F. Takahashi, W. Yin, and A. H. Guth, *Phys. Rev. D* **98**, 015042 (2018), 1805.08763.
- [70] G. Alonso-Álvarez, T. Hugle, and J. Jaeckel, *JCAP* **02**, 014 (2020), 1905.09836.
- [71] S. Nakagawa, F. Takahashi, and W. Yin, *JCAP* **05**, 004 (2020), 2002.12195.
- [72] S.-Y. Ho, F. Takahashi, and W. Yin, *JHEP* **04**, 149 (2019), 1901.01240.
- [73] H. Matsui, F. Takahashi, and W. Yin, *JHEP* **05**, 154 (2020), 2001.04464.
- [74] A. Chatrchyan and G. Servant, *JHEP* **06**, 107 (2023), 2210.01148.